Multiwavelength fiber laser employing a nonlinear Brillouin optical loop mirror: experimental and numerical studies

Yijun Yuan, [1,2] Yong Yao, [1,*] Miao Yi, [2] Bo Guo, [1] and Jiajun Tian [1]

[1]*College of Electronic and Information Engineering, Shenzhen Graduate School, Harbin Institute of Technology, Shenzhen, Guangdong Province, 518055, China*

[2]*College of Physics Science and Engineering Technology, Yichun University, Yichun, Jiangxi Province, 336000, China*

** yaoyong@hit.edu.cn*

Abstract: We numerically and experimentally study a multiwavelength fiber laser (MWFL) employing a nonlinear Brillouin optical loop mirror (NBOLM). Taking into account the impact of stimulated Brillouin scattering (SBS) effect on nonlinear polarization evolution, we present the power transmission equation of Stokes lines from the NBOLM. Thereafter, we combine the power transmission equation, coupled wave equations of SBS process in NBOLM, rate and power propagation equations in the erbium-doped fiber (EDF) to build up a model for the MWFL. Using this model, we can explain the impacts of EDF pump power, input polarization state and quarter-wave-plate angle on the number and amplitude flatness of output Stokes lines. Furthermore, the results from numerical calculations are verified by the experimental measurements.

OCIS codes: (140.3500) Lasers, erbium; (290.5900) Scattering, stimulated Brillouin.

References and links

1. K. J. Zhou, D. Y. Zhou, F. Z. Dong, and N. Q. Ngo, "Room-temperature multiwavelength erbium-doped fiber ring laser employing sinusoidal phase-modulation feedback," Opt. Lett. **28**(11), 893–895 (2003).
2. J. N. Maran, S. L. Rochelle, and P. Besnard, "C-band multi-wavelength frequency-shifted erbium-doped fiber laser," Opt. Commun. **218**(1–3), 81–86 (2003).
3. P. H. Wang, D. M. Weng, K. Li, Y. Liu, X. C. Yu, and X. J. Zhou, "Multi-wavelength Erbium-doped fiber laser based on four-wave-mixing effect in single mode fiber and high nonlinear fiber," Opt. Express **21**(10), 12570–12578 (2013).
4. Z. Q. Luo, M. Zhou, Z. P. Cai, C. C. Ye, J. Weng, G. Huang, and H. Xu, "Graphene-assisted multiwavelength erbium-doped fiber ring laser," IEEE Photon. Technol. Lett. **23**(8), 501–503 (2011).
5. J. J. Tian, Y. Yao, Y. X. Sun, X. L. Yu, and D. Y. Chen, "Multiwavelength Erbium-doped fiber laser employing nonlinear polarization rotation in a symmetric nonlinear optical loop mirror," Opt. Express **17**(17), 15160–15166 (2009).
6. X. S. Liu, L. Zhan, S. Y. Luo, Z. C. Gu, J. M. Liu, Y. X. Wang, and Q. S. Shen, "Multiwavelength erbium-doped fiber laser based on a nonlinear amplifying loop mirror assisted by un-pumped EDF," Opt. Express **20**(7), 7088–7094 (2012).
7. T. V. A. Tran, K. Lee, S. B. Lee, and Y. G. Han, "Switchable multiwavelength erbium doped fiber laser based on a nonlinear optical loop mirror incorporating multiple fiber Bragg gratings," Opt. Express **16**(3), 1460–1465 (2008).
8. X. H. Feng, H. Y. Tam, H. Liu, and P. K. A. Wai, "Multiwavelength erbium-doped fiber laser employing a nonlinear optical loop mirror," Opt. Commun. **268**(2), 278–281 (2006).
9. Z. X. Zhang, L. Zhan, K. Xu, J. Wu, Y. X. Xia, and J. T. Lin, "Multiwavelength fiber laser with fine adjustment, based on nonlinear polarization rotation and birefringence fiber filter," Opt. Lett. **33**(4), 324–326 (2008).
10. H. Lin, "Waveband-tunable multiwavelength erbium-doped fiber laser," Appl. Opt. **49**(14), 2653–2657 (2010).
11. Z. Chen, S. Ma, and N. K. Dutta, "Multiwavelength fiber ring laser based on a semiconductor and fiber gain medium," Opt. Express **17**(3), 1234–1239 (2009).
12. J. Yao, J. P. Yao, Z. C. Deng, and J. Liu, "Investigation of room-temperature multiwavelength fiber-ring laser that incorporates an SOA-based phase modulator in the laser cavity," J. Lightwave Technol. **23**(8), 2484–2490 (2009).

#210273 - $15.00 USD Received 15 Apr 2014; revised 7 Jun 2014; accepted 11 Jun 2014; published 17 Jun 2014

13. Y. G. Han, T. V. A. Tran, S. H. Kim, and S. B. Lee, "Development of a multiwavelength Raman fiber laser based on phase-shifted fiber Bragg gratings for long-distance remote-sensing applications," Opt. Lett. **30**(10), 1114–1116 (2005).
14. Z. Q. Luo, Z. P. Cai, J. F. Huang, C. C. Ye, C. H. Huang, H. Y. Xu, and W. D. Zhong, "Stable and spacing-adjustable multiwavelength Raman fiber laser based on mixed-cascaded phosphosilicate fiber Raman linear cavity," Opt. Lett. **33**(14), 1602–1604 (2008).
15. T. F. S. Büttner, I. V. Kabakova, D. D. Hudson, R. Pant, E. Li, and B. J. Eggleton, "Multi-wavelength gratings formed via cascaded stimulated Brillouin scattering," Opt. Express **20**(24), 26434–26440 (2012).
16. M. H. Al-Mansoori and M. A. Mahdi, "Multiwavelength L-band Brillouin-erbium comb fiber laser utilizing nonlinear amplifying loop mirror," J. Lightwave Technol. **27**(22), 5038–5044 (2009).
17. Y. G. Shee, M. H. Al-Mansoori, A. Ismail, S. Hitam, and M. A. Mahdi, "Multiwavelength Brillouin-erbium fiber laser with double-Brillouin-frequency spacing," Opt. Express **19**(3), 1699–1706 (2011).
18. Z. A. Rahman, S. Hitam, M. H. Al-Mansoori, A. F. Abas, and M. A. Mahdi, "Multiwavelength Brillouin fiber laser with enhanced reverse-S-shaped feedback coupling assisted by out-of-cavity optical amplifier," Opt. Express **19**(22), 21238–21245 (2011).
19. Y. J. Song, L. Zhan, J. H. Ji, Y. Su, Q. H. Ye, and Y. X. Xia, "Self-seeded multiwavelength Brillouin-erbium fiber laser," Opt. Lett. **30**(5), 486–488 (2005).
20. Y. J. Yuan, Y. Yao, J. J. Xiao, Y. F. Yang, J. J. Tian, and C. Liu, "Experimental and numerical study of high order Stokes lines in Brillouin-erbium fiber laser," J. Appl. Phys. **115**(4), 043102 (2014).
21. D. Stepanov and G. Cowle, "Modeling of multi-line Brillouin/erbium fiber lasers," Opt. Quantum Electron. **31**(5/7), 481–494 (1999).
22. H. A. Al-Asadi, M. H. Abu Bakar, M. H. Al-Mansoori, F. R. Adikan, and M. A. Mahdi, "Analytical analysis of second-order Stokes wave in Brillouin ring fiber laser," Opt. Express **19**(25), 25741–25748 (2011).
23. E. A. Kuzin, N. Korneev, J. W. Haus, and B. Ibarra-Escamilla, "Theory of nonlinear loop mirrors with twisted low-birefringence fiber," J. Opt. Soc. Am. B **18**(7), 919–925 (2001).
24. O. Pottiez, E. A. Kuzin, B. Ibarra-Escamilla, and F. M. Martínez, "Theoretical investigation of the NOLM with highly twisted fibre and a $\lambda/4$," Opt. Commun. **254**(1–3), 152–167 (2005).
25. G. P. Agrawal, *Nonlinear Fiber Optics* (Academic Press, 2007).
26. X. C. Xu, Y. Yao, and D. Y. Chen, "Numerical analysis of multiwavelength erbium-doped fiber ring laser exploiting four-wave mixing," Opt. Express **16**(16), 12397–12402 (2008).
27. M. H. Al-Mansoori and M. A. Mahdi, "Reduction of gain depletion and saturation on a Brillouin-erbium fiber laser utilizing a Brillouin pump preamplification technique," Appl. Opt. **48**(18), 3424–3428 (2009).

1. Introduction

Multiwavelength fiber lasers (MWFLs) have aroused considerable interest due to their potential applications in optical fiber sensing, microwave photonics and dense wavelength division multiplexing (DWDM) systems over the past years. Various approaches and mechanisms have been proposed to obtain multiwavelength operation in a fiber laser, such as frequency- or phase-shifted feedback [1, 2], four-wave mixing [3, 4], nonlinear optical loop mirror (NOLM) [5–8], nonlinear polarization rotation [9, 10], semiconductor optical amplifier [11, 12], Raman amplifier [13, 14] and stimulated Brillouin scattering (SBS) [15–20]. Among these approaches, the MWFLs based on SBS or NOLM are particularly attractive for their simple configuration, narrow linewidth (by utilizing SBS effect) and flat output amplitude (by utilizing NOLM effect). However, the MWFLs based on SBS effect have large amplitude divergence between low- and high-order Stokes lines. These lasers also have inconvenient tunability for the output Stokes lines (such as varying the erbium-doped fiber (EDF) pump power to adjust their number) [15–18]. On the other hand, MWFLs based on NOLM have unsatisfied stability and linewidth during the process of multiwavelength operation [5]. Inspired by their respective problems, we propose the combination of NOLM and SBS effects to achieve nonlinear Brillouin optical loop mirror (NBOLM) in a MWFL. The output Stokes lines of this MWFL have narrow linewidth, adjustable flatness of amplitude, and simple tunability of number. Moreover, we derive a model based on the equations from models of MBEFL in [20–22] and NOLM in [23, 24] to explain the operation mechanism of the MWFL employing a NBOLM.

In this paper, we build up the NBOLM function by injecting a Brillouin pump (BP) light signal into a coil of single mode fiber (SMF) in the NOLM. Due to the SBS effect, the fiber laser can achieve extremely narrow linewidth and rigid multiwavelength channels spacing. At the same time, its NOLM effect acts as an amplitude-equalizer to optimize the output

#210273 - $15.00 USD Received 15 Apr 2014; revised 7 Jun 2014; accepted 11 Jun 2014; published 17 Jun 2014

performance of Stokes lines and an intensity dependent loss to adjust the number of output Stokes lines in the fiber laser [5]. By considering the influence of SBS effect on nonlinear polarization evolution (NPE) in this NBOLM, we derive its power transmission equations of Stokes lines. Then, we combine these power transmission equations from NBOLM and rate and power propagation equations in EDF to build up a model for the MWFL employing a NBOLM. By utilizing this model, we numerically demonstrate how the number and amplitude flatness of output Stokes lines depend on input polarization state A_s^{cw}, quarter-wave plate (QWP) angle α and EDF pump power P_{EP}. Thereafter, we experimentally validate the numerical results and these two results are well in agreement.

2. Theory and experimental setup of the MWFL employing a NBOLM

Figure 1 illustrates the proposed MWFL configuration. It consists of EDF, optical circulator, two optical couplers, WDM, 1480 pump laser diode, tunable laser source (TLS) and NBOLM. The NBOLM is formed by a highly twisted SMF, a quarter-wave plate, a polarization controller (PC), and a 3 dB optical coupler. The 15 m EDF pumped by the 1480 nm laser diode provides the linear gain. The 20 km highly twisted SMF in the NBOLM is used as Brillouin gain with effective cross section area of 50 μm^2. Circulator is used to ensure unidirectional propagation of the light signals and decreases the noise. The TLS acts as the BP light signal and injects into the cavity via the 20% port of Coupler (80/20). Measured results are extracted from the system by using a 90/10 coupler at one output port of the NBOLM. The 10% port of this coupler is connected to the OSA for monitoring the output spectrum. The 90% port output to a power meter for measuring the total power of all the Stokes lines.

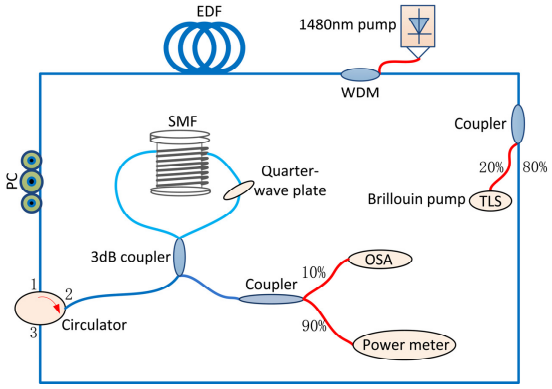

Fig. 1. Schematic diagram of the proposed fiber laser.

Firstly, to exploit the model of MWFL based on a NBOLM, we shall further develop the lump model proposed in [20], which consists of coupled wave equations of SBS for SMF and rate and propagation equations for EDF. However, the SMF of this MWFL is in a NBOLM which provides SBS effect and NPE effect (the QWP provides different nonlinear evolutions through the polarisation difference in the power-symmetric structure) simultaneously. These two effects can interplay with each other in the NBOLM. Therefore, instead of being described by coupled wave equations of SBS solely, the SMF in the NBOLM is described by the coupled wave equations for SBS process [21, 22] and NPE [23, 24]:

$$\frac{dP_{Bp\_n}^{cw/ccw}(z)}{dz} = -\frac{g_B}{A_{eff}} P_{Bp\_n}^{cw/ccw}(z) P_{S\_n}^{cw/ccw}(z), \qquad (1)$$

#210273 - $15.00 USD Received 15 Apr 2014; revised 7 Jun 2014; accepted 11 Jun 2014; published 17 Jun 2014

$$\frac{dP_{S\_n}^{cw/ccw}(z)}{dz} = -\frac{g_B}{A_{eff}} P_{Bp\_n}^{cw/ccw}(z) P_{S\_n}^{cw/ccw}(\mathrm{z}). \tag{2}$$

$$i\partial_s S_{Bp\_n}^{cw/ccw+} = [-\mu - \frac{1}{2}(3 - A_{S\_Bp\_n}^{cw/ccw})\,\mathrm{P}_{Bp\_n}^{cw/ccw}(\mathrm{z})] S_{Bp\_n}^{cw/ccw+}, \tag{3}$$

$$i\partial_s S_{Bp\_n}^{cw/ccw-} = [+\mu - \frac{1}{2}(3 + A_{S\_Bp\_n}^{cw/ccw})\,\mathrm{P}_{Bp\_n}^{cw/ccw}(\mathrm{z})] S_{Bp\_n}^{cw/ccw-}, \tag{4}$$

where the superscripts cw and ccw represent the clockwise and counterclockwise light beams, respectively. g_B and A_{eff} are Brillouin gain coefficient and effective cross section area, respectively. $P_{Bp\_n}^{cw/ccw}$ is the pump power to generate the n-order Stokes line with power $P_{S\_n}^{cw/ccw}$ in the SMF. Similarly, $P_{S\_n}^{cw/ccw}$ is the pump power $P_{Bp\_n+1}^{cw/ccw}$ to excite the (n + 1)-order Stokes line with power $P_{S\_n+1}^{cw/ccw}$. In other words, $P_{Bp\_n}^{cw/ccw}$ is $P_{S\_n-1}^{cw/ccw}$. In Eqs. (3) and (4), $\mathrm{S}_{Bp\_n}^{cw/ccw+}$ and $\mathrm{S}_{Bp\_n}^{cw/ccw-}$ are the elliptical right and left polarization eigenmodes of the n-order BP light signal, respectively. $A_{S\_Bp\_n}^{cw/ccw} = \left|S_{Bp\_n}^{cw/ccw+}\right|^2 - \left|S_{Bp\_n}^{cw/ccw-}\right|^2$ is a constant during the propagation of n-order BP light wave [also (n-1)-order Stokes line]. In the case of high twisted SMF, eigenmodes $[S_{Bp\_n}^{cw/ccw+}, S_{Bp\_n}^{cw/ccw-}]$ match approximately with circular polarization states $[C_{Bp\_n}^{cw/ccw+}, \mathrm{C}_{Bp\_n}^{cw/ccw-}]$. $\mu = \sqrt{\pi^2 + g^2}$, where $g = \gamma\pi / k$ is the ratio of circular to linear birefringence, $k = \pi / \mathrm{L}_b$ describing the linear birefringence, and $\gamma = [h0/(2n) - 1]q$ the circular birefringence. Furthermore, L_b is the beat length of SMF, n the refractive index and $h0 \approx 0.13 - 0.16$ for the silica fiber, q the twist rate. $P_{Bp\_n}^{cw/ccw}(z) = b\pi P_{in\_n}(\mathrm{z}) / k$ is the normalized power, where $b = 4\pi\tilde{n}_2 / 3\lambda A_{eff}$ is the nonlinearity ($\tilde{n}_2$ the Kerr coefficient, and λ the wavelength of Stokes line).

Equations (1)-(4) indicate that the power $P_{Bp\_n}^{cw/ccw}(z)$ varies with distance of the highly twisted SMF due to the SBS effect. To achieve the transfer matrix for Eqs. (3) and (4), we divide the highly twisted SMF into t spans ($t = 10000$ in the numerical simulation) as shown in Fig. 2. The initial input power P_{in_1} (from the TLS) is divided into clockwise light signal with power $P_{Bp\_1}^{cw}$ and counterclockwise light signal with power $P_{Bp\_1}^{ccw}$ by the 3 dB coupler. These two signals input in the 1st SMF span with powers $P_{Bp\_1,1}^{cw}$ and $P_{Bp\_1,1}^{ccw}$ to generate the corresponding 1-order Stokes line with powers $P_{S\_1,1}^{cw}$ and $P_{S\_1,1}^{ccw}$. Although the directions of $P_{Bp\_1,1}^{cw}$ and $P_{S\_1,1}^{cw}$ are in opposite direction, we take the same superscripts for simplicity (the same applies to the other Stokes lines). Then the 2nd SMF span with input powers $P_{Bp\_1,2}^{cw}$ and $P_{Bp\_1,2}^{ccw}$ generates the corresponding Stokes lines respectively with powers $P_{S\_1,2}^{cw}$ and $P_{S\_1,2}^{ccw}$, and so on. Lastly, at the 10000th SMF span, the generated cw ($P_{S\_1,10000}^{cw}$) and ccw ($P_{S\_1,10000}^{ccw}$) 1-order Stokes lines are coupled in the 3 dB coupler. This coupled 1-order Stokes line outputs from port 1 of the 3 dB coupler and is amplified by the EDF, then inputs into the NBOLM again as the next round-trip initial power P_{in_1}. This round-trip process repeats till the MWFL is in a steady state and there is no power variation for the Stokes lines. During this round-trip process, $P_{Bp\_n}^{cw/ccw}(z)$ in each fiber span (a small length Δl) is regarded as

#210273 - $15.00 USD Received 15 Apr 2014; revised 7 Jun 2014; accepted 11 Jun 2014; published 17 Jun 2014

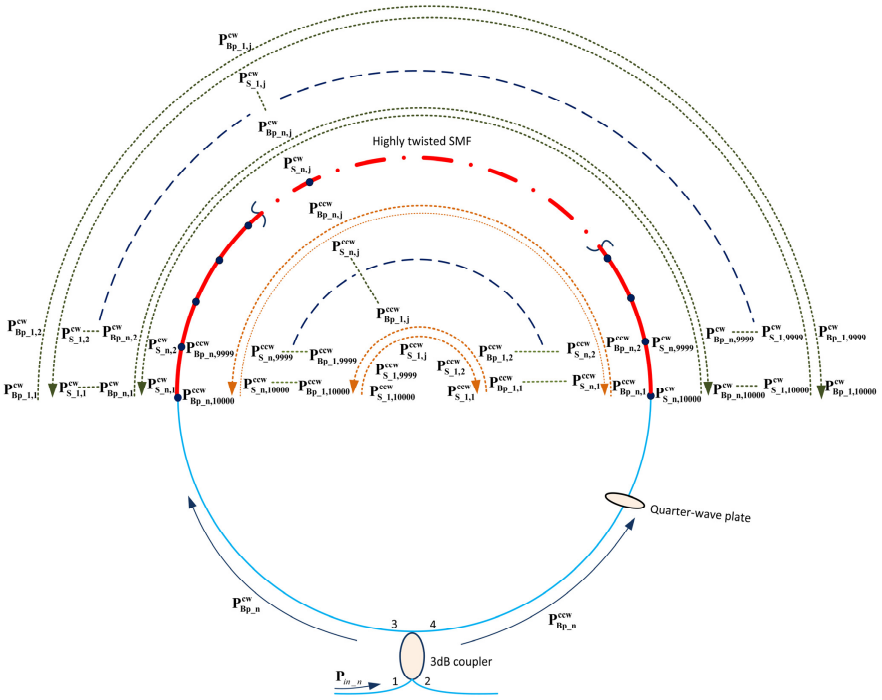

Fig. 2. Operation mechanism scheme of the NBOLM.

a fixed parameter. Therefore, Eqs. (3) and (4) can be solved by a integration technique similarly as in [24]. From the derivation based on Eqs. (3) and (4), we can write down the transfer matrix of one highly twisted SMF span for the (n-1)- order Stokes line as:

$$F_{Bp\_n,j}^{cw/ccw}=\begin{bmatrix} e^{i[\mu+\frac{1}{2}(3-A_{S\_Bp\_n}^{cw/ccw})P_{Bp\_n,j}^{cw/ccw}]\Delta l} & 0 \\ 0 & e^{i[-\mu+\frac{1}{2}(3+A_{S\_Bp\_n}^{cw/ccw})P_{Bp\_n,j}^{cw/ccw}]\Delta l} \end{bmatrix} \tag{5}$$

where the subscript j describes the j-th SMF span. Therefore, the transfer matrix of the total highly twisted SMF (divided in t spans) for the (n-1)-order Stokes line (with power $P_{S\_n-1}^{cw/ccw}$ or $P_{Bp\_n}^{cw/ccw}$) is

$$\begin{aligned} F_{Bp\_n}^{cw/ccw} &= F_{Bp\_n,1}^{cw/ccw}\times F_{Bp\_n,2}^{cw/ccw}\times\cdots\times F_{Bp\_n,\mathrm{j}}^{cw/ccw}\times\cdots\times F_{Bp\_n,t}^{cw/ccw} \\ &= \begin{bmatrix} e^{i[\mathrm{k}\,\mu+\frac{1}{2}(3-A_{S\_Bp\_n}^{cw/ccw})\sum_{j=1}^{t}P_{Bp\_n,j}]\Delta l} & 0 \\ 0 & e^{i[-\mathrm{k}\,\mu+\frac{1}{2}(3+A_{S\_Bp\_n}^{cw/ccw})\sum_{j=1}^{t}P_{Bp\_n,j}]\Delta l} \end{bmatrix} \end{aligned} \tag{6}$$

Based on the eigenmodes $[C_{Bp\_n}^{cw/ccw+}, C_{Bp\_n}^{cw/ccw-}]$, the transfer matrix of the QWP can be written as:

$$QWP_{Bp\_n}^{cw/ccw}=\begin{bmatrix} \frac{1+i}{2} & \frac{1-i}{2}e^{2i\alpha/-2i\alpha} \\ \frac{1-i}{2}e^{-2i\alpha/2i\alpha} & \frac{1+i}{2} \end{bmatrix} \tag{7}$$

where α is the QWP angle defined in a frame (not the rotating frame and its y-axis is perpendicular to the plane of NBOLM). The divergence of frame between QWP and the fiber is described by the matrix

#210273 - $15.00 USD Received 15 Apr 2014; revised 7 Jun 2014; accepted 11 Jun 2014; published 17 Jun 2014

$$\Theta_{Bp\_n}^{cw/ccw} = \begin{bmatrix} e^{i\theta} & 0 \\ 0 & e^{-i\theta} \end{bmatrix} \tag{8}$$

where $\theta = kq\Delta l$ is the total twist of fiber and Δl is the length of every twisted SMF span. After some calculations as described in [24].The power transmission of the NBOLM is

$$T_{Bp\_n} = \frac{1}{2} - \frac{1}{2}\cos(\beta - 2\alpha - \frac{1}{2}A_{s\_Bp\_n}^{cw}\sum_{j=1}^{t} P_{Bp\_n,j}\Delta l)\cos(\beta - 2\alpha - \frac{1}{2}A_{s\_Bp\_n}^{ccw}\sum_{j=1}^{t} P_{Bp\_n,j}\Delta l). \tag{9}$$

Here $A_{s\_Bp\_n}^{ccw} = -\sqrt{1-(A_{s\_Bp\_n}^{cw})^2}\sin 2(\alpha+\psi)$, and A_s^{cw} represents the input polarization state and $\beta = k\mu\Delta l + \theta$. In the MWFL based on the NBOLM, the effect of EDF can be described by the rate and propagation equations as in [20]. The SBS threshold of the twisted SMF in the NBOLM is approximately [25]

$$P_{th} \approx 21A_{eff} / (g_B L_{eff}). \tag{10}$$

Similarly, the steady state equation of this fiber laser can be built with no power-variation for P_{Bp_n} [26]:

$$P_{Bp\_n}^{m} = F_{EDF} \times F_{NBOLM} \times F_{Loss} \times P_{Bp\_n}^{m-1}. \tag{11}$$

where F_{EDF}, F_{NBOLM} and F_{Loss} represent the effects of EDF, NBOLM, and the total cavity loss of the laser, respectively. Notice that $P_{Bp\_n}^{m}$ dictates the m-th round-trip power of the (n-1)-order Stokes line in the MWFL.

3. Numerical results and discussion

We perform series of numerical simulations by the proposed model in Section 2. The parameters for rate and propagation equations described in [20] are $g_B = 3\times10^{-12}\ m/W$, $h = 6.63\times10^{-34}\ J\cdot s$, $N = 3\times10^{25}/m^3$ (the total Er^{3+} ion density in the EDF), $\tau_{21} = 10^{-2}$ s, $N_{2\_initial} = 10^{10}/m^3$ (the initial second energy state population density in the EDF), $\Delta\nu = 5\times10^{10}\ Hz$, $\xi_{pe} = 0$, $\xi_{pa} = 3.28\times10^{-25}\ m^2$, $c = 3\times10^8\ m/s$. ξ_{se} and ξ_{sa} of different frequency (wavelength) are achieved by curve fitting method. The other chosen parameters are $L_{EDF} = 15\ m$, $L_{SMF} = 20\ km$ (the long SMF provides a low SBS threshold and more obvious nonlinearity effect for this fiber laser), $A_{eff} = 50\ \mu m^2$ (EDF and twisted SMF fiber), $n = 1.45$, $q = 6$ turn/m, $h0 = 0.14$, $L_b = 15\ m$, $\tilde{n}_2 = 3.2\times10^{-20}$ and $\lambda_{EP} = 1480\ nm$. $P_{s\_1}^{cw/ccw}(L_{SMF})$ is a very small quantity of the SBS noise ($\approx 6\times10^{-9}$ W) for seeding each Stokes line at the other end of the SMF. The total cavity loss is $F_{Loss} = 16\ dB$ which is fairly large because the experimental configuration using many fiber connectors, a long SMF and NOLM structure induces extra loss. The Stokes lines circulate in the round-trips as governed by the rate and propagation equations, SBS Eqs. (1) and (2), and power transmission Eq. (9). By utilizing Eq. (11), the steady state of this fiber laser can be determined.

Figure 3 demonstrates how the calculated number of output Stokes lines depends on the EDF pump power P_{EP} when $P_{Bp\_1} = 3\ mW$ and $\lambda_{Bp\_1} = 1558.42\ nm$. Due to the free-running oscillation center wavelength of this fiber laser is around 1558.5 nm, we choose the BP wavelength around 1558.5 nm to obtain more output Stokes lines. It is noticed that the center wavelength is decided by Er^{3+} concentration, cavity loss and EDF length. In Fig. 3(a), the EDF

#210273 - $15.00 USD Received 15 Apr 2014; revised 7 Jun 2014; accepted 11 Jun 2014; published 17 Jun 2014

pump power P_{EP} is taken to be 35 mW, below the laser threshold (about 62 mW for $\alpha = 120^o$ and $A_s^{cw} = 0.36$) for outputting Stokes line. In such case, Stokes line is not expected. When P_{EP} increases to 126 mW which is in excess of the cavity loss and satisfies the lasing condition of a fiber laser, 6 Stokes lines occur with a channel spacing of 0.08 nm as shown in Fig. 3(b). Similarly, further increasing P_{EP} to 265 mW and 348 mW as depicted in Figs. 3(c) and 3(d), 13 and 16 Stokes lines are generated, still with a constant spacing 0.08 nm, respectively. As a result, the number of output Stokes lines increases with P_{EP} in this MWFL based on a NBOLM. This is because that a high P_{EP} provides a large amount of excited Er^{3+} ions for Stokes lines in the EDF. More Stokes lines acquire these excited Er^{3+} ions, and exceed the cavity loss and come out from this fiber laser.

It is noticed that the output power of every Stokes lines in this fiber laser are very low (usually below −30dBm in the numerical results or the following experimental results). This is because we use a very long SMF, many connectors and 10% power extracted from the system by a 90/10 coupler. The large enough amplified BP light signal passes through the SMF and generates Stokes lines. The power of the residual BP light signal and the Stokes lines is around the SBS threshold of the SMF (several dBm SBS threshold for 20km SMF) after the SBS effect. This is because if these powers larger than the SBS threshold, the extra power can transfer to the other Stokes line or generate a new one. These Stokes lines decrease to about −20dBm at the input port of the 90/10 coupler due the loss of the components ($\approx$ 7dB for SMF, $\approx 3 \sim 8$dB for NOLM structure, $\approx$ 7dB for connectors and other components). Thereafter, due to the 10% port of the 90/10 coupler, the output power is about −30dBm. The ASE of EDF and the spontaneous Brillouin scattering in the SMF are ignored due to the large cavity loss.

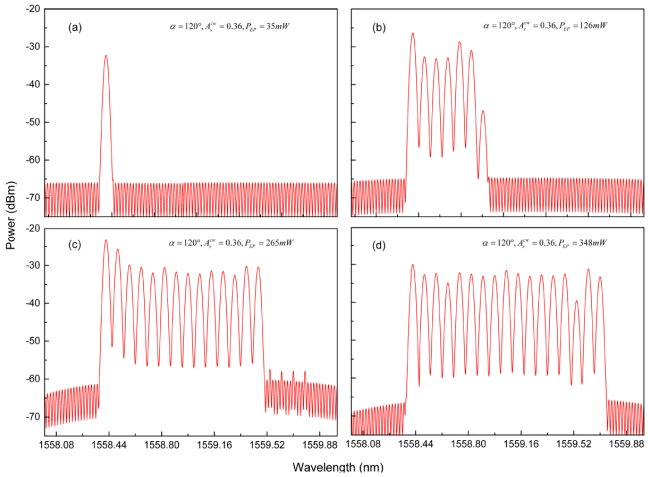

Fig. 3. Numerical simulation spectra for different P_{EP} : (a) $P_{EP} = 35\,mW$, (b) $P_{EP} = 126\,mW$, (c) $P_{EP} = 265\,mW$, (d) $P_{EP} = 348\,mW$.

To clearly explain the mechanism of the input polarization state A_s^{cw} and QWP angle α on the number and amplitude of output Stokes lines, we calculate the reflection of NBOLM which varies with the input power as shown in Fig. 4. As seen in Fig. 4(a), as α increase from 126^o to 132^o with a fixed $A_s^{cw} = 0.21$, the reflection of NBOLM decreases (from dotted line to dashed line). Specially, when we increase A_s^{cw} from 0.18 to 0.21 with a fixed $\alpha = 132^o$, the slope of the reflection lines grows slightly (from solid line to dashed line). However, when we

#210273 - $15.00 USD Received 15 Apr 2014; revised 7 Jun 2014; accepted 11 Jun 2014; published 17 Jun 2014

vary A_s^{cw} and α simultaneously, the reflection of the NBOLM and its slopes change in a relative larger amount as shown in Fig. 4(b).

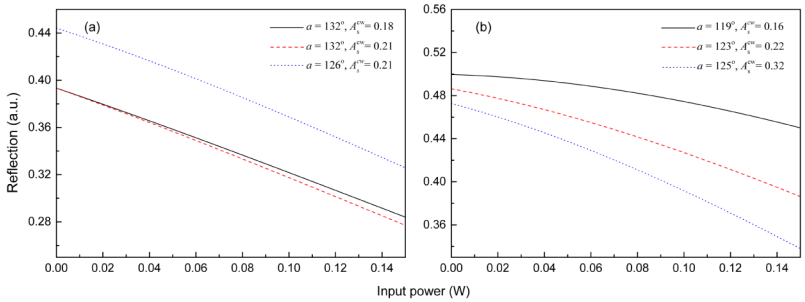

Fig. 4. Calculated reflection of the NBOLM for different A_s^{cw} and α : (a) varied A_s^{cw} or α , (b) varying A_s^{cw} and α simultaneously.

Figure 5 shows the numerical calculated impact of input polarization state A_s^{cw} and the QWP angle α on the number of output Stokes lines for $P_{Bp\_1} = 3\,mW$, $\lambda_{Bp\_1} = 1557.92\,nm$ and $P_{EP} = 181\,mW$. In Figs. 5(a) and 5(b), taking $\alpha = 132^o$ and $A_s^{cw} = 0.21$, we achieve 2 Stokes lines. By decreasing A_s^{cw} to 0.18 , there is 3 Stokes lines occur in this fiber laser. As seen in Figs. 5(c) and 5(d), we take $\alpha = 129^o$ and $\alpha = 126^o$ for $A_s^{cw} = 0.21$, 5 and 7 Stokes lines can emerge, respectively. The reason is that the decrease of A_s^{cw} or α can increase the reflection of the Stokes lines as shown in Fig. 4(a). It means that more power of the Stokes lines are reflected back into the cavity. In such case, the total cavity loss of the Stokes lines decreases. Therefore, more Stokes lines have power exceeding the threshold of the fiber laser and lasing out. Noticed that the variation of A_s^{cw} changes the reflection of NBOLM slightly, and the increase of number for output Stokes lines is not obvious.

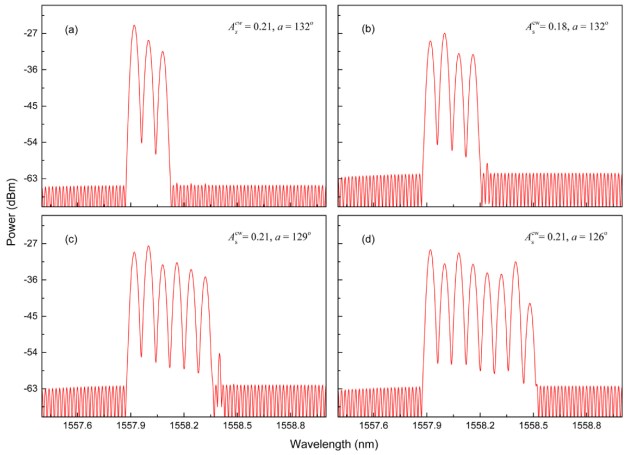

Fig. 5. Numerical simulation spectra for different A_s^{cw} or α : (a) $A_s^{cw} = 0.21, \alpha = 132^o$, (b) $A_s^{cw} = 0.18, \alpha = 132^o$, (c) $A_s^{cw} = 0.21, \alpha = 129^o$, (d) $A_s^{cw} = 0.21, \alpha = 126^o$.

Figure 6 depicts the calculated influence of the input polarization state A_s^{cw} and the QWP angle α on the amplitude flatness of Stokes lines for $P_{Bp\_1} = 3\,mW$, $\lambda_{Bp\_1} = 1558.42\,nm$

#210273 - $15.00 USD Received 15 Apr 2014; revised 7 Jun 2014; accepted 11 Jun 2014; published 17 Jun 2014

and $P_{EP} = 181\,mW$. It is seen that the largest amplitude divergence of the Stokes lines (15 channels) is almost 18 dB for $\alpha = 119^o$, $A_s^{cw} = 0.16$. Slightly varying PC and the QWP angle to a position of $\alpha = 123^o$ and $A_s^{cw} = 0.22$, the amplitude variation of the Stokes lines (11 channels) decrease to 2 dB, as depicted in Fig. 6(b). This is because the slope of reflection line changes with varying both A_s^{cw} and α as shown in Fig. 4(b). By finely adjusting A_s^{cw} and α, the net gain of more Stokes lines are approximately equal. Therefore, the amplitudes of these Stokes lines become nearly the same.

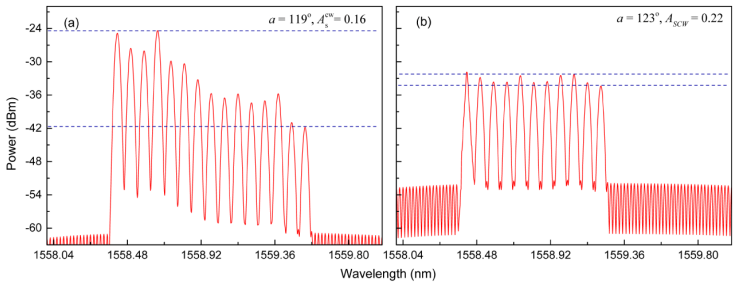

Fig. 6. Numerical simulation spectra for varying A_s^{cw} and α simultaneously: (a) $\alpha = 119^o, A_s^{cw} = 0.16$, (b) $\alpha = 123^o, A_s^{cw} = 0.22$.

4. Experimental validation

The numerical calculated impacts P_{EP}, A_s^{cw} and α on the number and amplitude of output Stokes lines are validated by our experimental results. Figure 7 demonstrates that the number of output Stokes lines vary with P_{EP}. Same as the previously calculated results (seen in Fig. 3), the number of output Stokes lines increases with P_{EP} for $\lambda_{Bp\_1} = 1558.42\,nm$, $P_{Bp\_1} = 3\,mW$

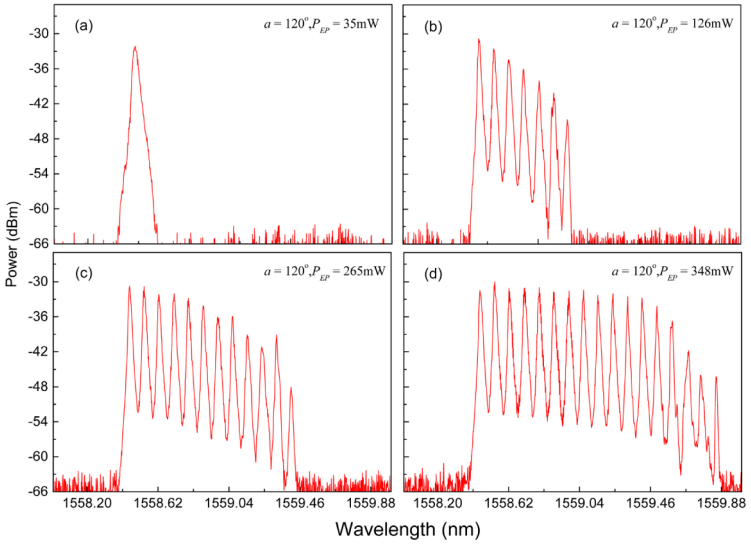

Fig. 7. Experimental output spectra for different P_{EP} : (a) $P_{EP} = 35\,mW$, (b) $P_{EP} = 126\,mW$, (c) $P_{EP} = 265\,mW$, (d) $P_{EP} = 348\,mW$.

#210273 - $15.00 USD Received 15 Apr 2014; revised 7 Jun 2014; accepted 11 Jun 2014; published 17 Jun 2014

and $\alpha = 120^o$ (a fixed A_s^{cw}). When $P_{EP} = 35\,mW$, there is only one channel lasing (BP light signal with no Stokes line). Increasing P_{EP} to $126mW$, we achieve 6 Stokes lines with a fixed spacing 0.08 nm as shown in Fig. 7(b). As we gradually increase P_{EP} to $265mW$ and $348mW$, respectively, 11 [seen in Fig. 7(c)] and 16 Stokes lines [seen in Fig. 7(d)] occur in the fiber laser, all with a constant spacing 0.08 nm. It is noticed that the number of output Stokes lines in this work (around 16) is much lower than the number in [27]. The main reason is that we use many connectors and the long SMF induce a large cavity loss.

Figure 8 shows the experimental results that the number of Stokes lines depends on A_s^{cw} and α individually with $\lambda_{Bp\_1} = 1557.92\,nm$, $P_{Bp\_1} = 3\,mW$ and $P_{EP} = 181\,mW$ (similar to the numerical results in Fig. 5). As shown in Figs. 8(a) and 8(b), the Stokes lines increase from 2 to 3 by only adjusting the PC from state 1 to state 2 with $\alpha = 132^o$. Similarly, the Stokes lines increase from 5 to 6 by solely decreasing α from 129^o to 126^o with a fixed A_s^{cw}. We note that the number of output Stokes lines make a little bit change by varying the PC state A_s^{cw} (the PC state is varied by adjusting the polarization controller and denotes with PC state 1 and 2 for different states A_s^{cw}). However, the variation of α change the number of output Stokes lines obviously. These are mainly resulted from the difference of the reflection variation from the NBOLM as shown in Fig. 4(a)

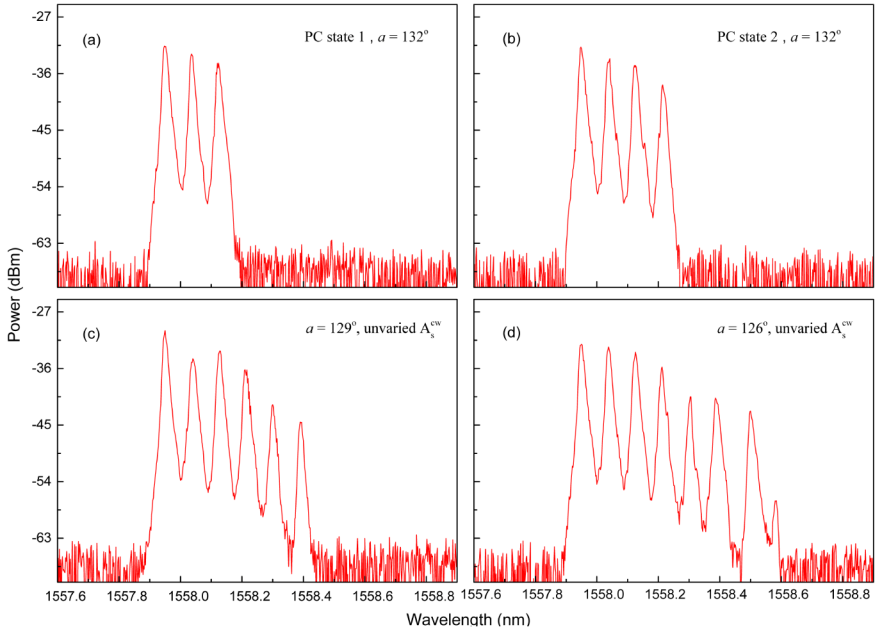

Fig. 8. Experimental output spectra for different A_s^{cw} or α : (a) PC state 1 and (b) PC state 2 for $\alpha = 132^o$, (c) $\alpha = 129^o$ and (d) $\alpha = 126^o$ for unvaried A_s^{cw}.

Furthermore, as we adjust both the PC state A_s^{cw} and QWP angle α finely, the amplitude flatness of the Stokes lines can be improved as shown in Fig. 9 (similar to numerical result in Fig. 6). When $\alpha = 122^o$ and A_s^{cw} in PC state 1, there are 5 Stokes lines in 3 dB power range as seen in Fig. 9(a). However, when $\alpha = 120^o$ and slightly adjusting PC to state 2, there are 11 Stokes lines in 3 dB power range as shown in Fig. 9(b). However, the total number of output

#210273 - $15.00 USD Received 15 Apr 2014; revised 7 Jun 2014; accepted 11 Jun 2014; published 17 Jun 2014

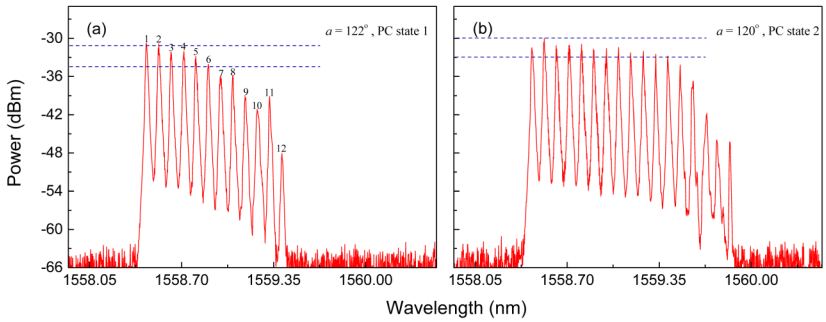

Fig. 9. Experimental output spectra for varying A_s^{cw} and α simultaneously: (a) PC state 1 with $\alpha = 122^o$, (b) PC state 2 with $\alpha = 120^o$.

Stokes lines mostly increase when α decreases (PC state can increases or decreases several output Stokes lines, but its effect is more weak than α) as shown in Fig. 9 (11 Stokes lines for $\alpha = 122^o$, 16 Stokes lines for $\alpha = 120^o$ in experimental results) and in Fig. 6 (10 Stokes lines for $\alpha = 123^o$, 14 Stokes lines for $\alpha = 119^o$ in numerical results). This is because α affects the reflection ratio more obviously and the input polarization state mainly affects the slope of the reflect lines. Due to the inaccuracy of manual adjustment of A_s^{cw} and α, it is difficult to achieve suitable positions of A_s^{cw} and α for a better amplitude flatness as predicted by the numerical results.

The power stability of this MWFL is also observed when $\alpha = 122^o$, A_s^{cw} in PC state 1, $\lambda_{Bp\_1} = 1558.42\ nm$, $P_{Bp\_1} = 3\ mW$ and $P_{EP} = 348\ mW$ [seen in Fig. 9(a)]. We scanned the output spectra every six minutes in an hour and found that the output power of the Stokes lines is very stable except the last output Stokes line in the spectra. The peak power variations of line 1-11 are all within $\pm 0.12\ dB$, as shown in Fig. 10. However the peak power of line 12 varies a little bitter, even sometimes hops with a next Stokes line (not included in Fig. 10 for its large instability). This is because the EDF gain for line 12 is under the saturation level. Therefore, the variation of EDF gain for this line results in its unstable peak power. When this power is sometimes beyond the threshold, the next Stokes line occurs.

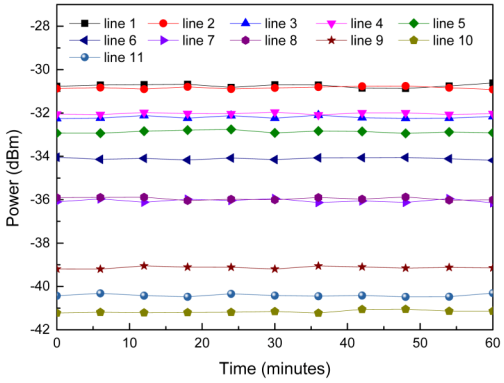

Fig. 10. Experimental peak power stability of the Stokes lines and Bp.

5. Conclusion

We have developed a model for the MWFL employing a NBOLM. It has ingredients of coupled wave equations of nonlinear polarization evolution and SBS process, rate and propagation

#210273 - $15.00 USD Received 15 Apr 2014; revised 7 Jun 2014; accepted 11 Jun 2014; published 17 Jun 2014

equations. This theoretical model successfully explains the influences of EDF pump power P_{EP}, input polarization state A_s^{cw} and QWP angle α on the number and amplitude flatness of output Stokes lines in this fiber laser. We can find an optimum P_{EP}, A_s^{cw} and α to improve the output performance of the MWFL. Alternatively, we have experimentally validated the theoretical predictions and measured the output power stability of the Stokes lines. The results from experimental observations compare favorably with the theoretical predictions. This MWFL with easily controlling number and flat amplitude of Stokes lines may be useful to facilitate the potential application of multiwavelength optical source in DWDM optical communication system.

Acknowledgments

This work is supported by National Natural Science Foundation of China (No. 61107036), and the Guangdong Province Shenzhen Municipal Science and Technology Plan (project Nos. JC201005260185A, JC201105160592A, JCYJ20120613114137248, JCYJ 20120613143649014, and KQCX20120801093710373), and Guangdong Province Ministry of Education Production-study-research Combination Project (2010B090400306).

#210273 - $15.00 USD Received 15 Apr 2014; revised 7 Jun 2014; accepted 11 Jun 2014; published 17 Jun 2014